Comparative Performance Analysis of PID and Sliding Mode Controllers in Speed Control of Induction Motor Drives with Intermittent Loading

ABSTRACT

Induction motor (IM) is the most used AC machine, and it is a constant speed device. If induction motion must be used in variable speed applications, its speed must be controlled. Speed control of a squirrel cage induction motor (SCIM) using a control algorithm with proportional integral derivative (PID) and sliding mode controller (SMC) was designed, simulated, and analyzed in this paper. Three-phase SCIM was considered, MATLAB software was used for both design and simulation and decoupling of the flux and torque-producing components for separate control was done for the actual control of the SCIM drive. The motor drive was used in driving a constant load of 0% (0 Nm), 28% (4 Nm), and 62% (12 Nm) of the rated torque with a variable speed of 0 rad/s, 10 rad/s, and 25 rad/s. It is observed that SMC gave the best speed performance compared to other controllers. The steady-state error, rise time, settling time, and overshoot of the SMC model were 0.1%, 0.01 sec, 0.05 sec, and 4%, respectively while that if PID were respectively 2 %, 0.02 sec, 0.2 sec, and 16 %, when driving 4Nm under intermittent speed. The improved speed performance of the proposed SM controller can be used in robotics where high precision speed performance is required.

Keywords: Induction motor; proportional integral derivative; sliding mode controller; vector control.

1. INTRODUCTION

Variable speed application is a trend in a lot of industrial processes, and AC machines are a key player in this process. AC machines are mostly a constant speed device, and this makes them unsuitable for this application. Induction motor (IM) is the most used AC machine, and it is a constant speed device. Speed control of IM is of great practical concern in many modern industrial operations where variable speed application is required. This is because IM has to satisfy variable speed characteristics requirements with minimize steady-state error, overshoot and undershoot suitable for variable speed operations within some microelectronic systems, and the control must have some economic benefits [1-8]. Industrial applications such as conveyors and robotics require variable-speed motoring mode, where different speed operations are carried out within the same system [9,10,11]. IM is always used for these applications because of its inherent characteristics. Variable Refrigerant Flow (VRF) technology uses variable speed drive applications to provide the needed comfort to occupants; it exhibits a 20–40% reduction in energy [12]. Some systems are powered by renewable energy sources like solar, wind, hydro, etc. The speed of machines used in driving loads within this system can be controlled for an effective response, and this can also improve system efficiency [13,14,15,16,17]. Technologies have made it possible to achieve efficient speed control with vector control

technique long with nonlinear [18–21]. Where conventional controllers like PID and nonlinear controllers like fuzzy logic and sliding mode and so on are employed to a realistic specific speed requirement in a given operating condition. For example, Kimiaghalam et al. [3] developed a model of induction motor drive for speed control using a hybrid controller consisting of proportional integral derivative (PID) and fuzzy logic, and the target load was a nonlinear load like a pump. The model gave an improved response when compared to either fuzzy logic or PID controller. In Oliveira and Uki [19], dynamic response using a fuzzy logic controller (FLC) was compared with a proportional integral (PI) controller; the latter showed superior performance at low speed. Umoette et al. [4] presented variable refrigerant flow (VRF) technology using variable speed drives. The results showed that the energy consumed by the VRF system was reduced by 40%. In Eissa et al. [22], particle swarm optimization (PSO) was used in getting an optimized value of specific speed, while Jayashri et al. [23] proposed a novel hybrid control of IM based on the combination of direct torque control (DTC) and genetic algorithm. The control method showed good performance at only one operating speed.A novel search algorithm was proposed in Souad et al. [24] and Umoette et al. [13] to improve the design of the FLC and FLC-PIC, respectively, for IM speed control. The proposed algorithm provides an easy approach for obtaining membership functions. The developed controller provided the needed stability and good dynamic response under speed and mechanical load change. Wang et al. [12] developed an optimized hybrid controller model for vector speed control technique on variable speed and intermittent loading operating conditions. The speed range considered was lower in the region of 5 to 30 rad/sec. The study was useful in the Lowe speed applications. Umoette et al. [14] studied the different methodologies of IM drives control. The study showed that speed, power, and efficiency of IM have been controlled by various techniques like frequency control, supply voltage control, and the multiple stator winding method. Implementation of indirect field oriented control (IFOC) on IM drive with PI control was presented in Umoette et al. [2], and the results show a good dynamic response on intermittent loading operating conditions. Umoette et al. [1] used a finite element analysis approach to obtain the dynamic performance of IM under intermittent loading conditions without control.

The simulation results showed the effect of different loads on the speed performance of the motor. Wang et al. [12] proposed a control technique that analyzed three different inverter modes (square wave, asynchronous, and synchronous).

The simulation results of the cited literature show that sensitive parameters like rise time, settling time, speed error, undershoots, overshoots, steady-state error, and load torque ripple of the IM drives are still high, which will not be accepted in many industrial applications. Also, stress in getting the optimal control parameters is much, especially in fuzzy logic controllers; hence, a sliding mode controller is developed in this work to suit a lot of operating conditions of an induction motor that will be discussed in this work. Hence, speed control of an IM still requires more research recognition, which will be considered in this paper.

The present study will focus on driving a squirrel cage IM (SCIM) with intermittent loading and variable seed control. The performance of the PID controller will be compared to that of the sliding mode controller in the listed operating conditions. The performance of these controllers will be assessed and compared. The study is expected to produce a SCIM model with improved speed performance characteristics compared to previous literature. Moreover, the proposed control algorithm will lead to improvements in variable applications like chillers, VRF technology, cranes, and robotics.

2. ANALYTICAL MODELLING OF SCIM

SCIM is an AC machine whose speed at loading conditions is always less than the synchronous speed, and it operates on the principle of electromagnetic induction.

The voltage equations of SCIM in dq0 axis using analytical method are given in equation (1) – (4):

$$v_{qs} = R_s i_{qs} + \frac{d\varphi_{qs}}{dt} + \omega_e \varphi_{ds} \quad (1)$$

$$v_{ds} = R_s i_{ds} + \frac{d\varphi_{ds}}{dt} - \omega_e \varphi_{qs} \quad (2)$$

$$v_{qr} = R_r i_{qr} + \frac{d\varphi_{qr}}{dt} + (\omega_e - \omega_r)\varphi_{dr} \quad (3)$$

$$v_{dr} = R_r i_{dr} + \frac{d\varphi_{dr}}{dt} - (\omega_e - \omega_r)\varphi_{qr} \quad (4)$$

and

$$v_{qr} = v_{dr} = 0$$

The flux equation:

$$\varphi_{qs} = L_{Is} i_{qs} + L_m(i_{qs} + i_{qr}) \quad (5)$$

$$\varphi_{qr} = L_{Ir} i_{qr} + L_m(i_{qs} + i_{qr}) \quad (6)$$

$$\varphi_{ds} = L_{Is} i_{ds} + L_m(i_{ds} + i_{dr}) \quad (7)$$

$$\varphi_{dr} = L_{Ir} i_{dr} + L_m(i_{ds} + i_{dr}) \quad (8)$$

where v_{qs} , v_{ds} are the applied voltages to the stator, i_{ds}, i_{qs}, i_{dr} , i_{qr} are the corresponding d and q axis stator current and rotor currents. $\varphi_{qs,}\varphi_{qr}$, φ_{ds}, φ_{dr} , are the rotor flux component, R_s , R_r are the stator and rotor resistances, L_{Is}, L_{Ir} denotes stator and rotor inductances, whereasL_m is the mutual inductance. Combining the flux equation with (1), (2), (3) and (4), the electrical transient model in term of voltage and current can be represents in matrix form as:

$$\begin{bmatrix} v_{qs} \\ v_{ds} \\ v_{qr} \\ v_{dr} \end{bmatrix} = \begin{bmatrix} R_s + SL_S & \omega_e L_S & SL_m & \omega_e L_m \\ -\omega_e L_S & R_s + SL_S & -\omega_e L_m & SL_m \\ SL_m & (\omega_e - \omega_r)L_m & R_s + SL_S & (\omega_e - \omega_r)L_r \\ -(\omega_e - \omega_r)L_m & SL_m & -(\omega_e - \omega_r)L_r & R_r + SL_r \end{bmatrix} \begin{bmatrix} i_{qs} \\ i_{ds} \\ i_{qr} \\ i_{dr} \end{bmatrix}$$

where, S is the Laplace operator. (9)

The electromagnetic torque equation given in equation (10)

$$T_e = \frac{3PL_m}{4L_r}(\varphi_{dr} i_{qs} - \varphi_{qr} i_{ds}) \quad (10)$$

where *P*, denote the pole number of the motor. If the vector control is fulfilled, the q component of the rotor field φ_{qr} would be zero. Then the electromagnetic torque is controlled only by q-axis stator current and is shown in equation (11)

$$T_e = \frac{3PL_m}{4L_r}(\varphi_{dr} i_{qs}) \quad (11)$$

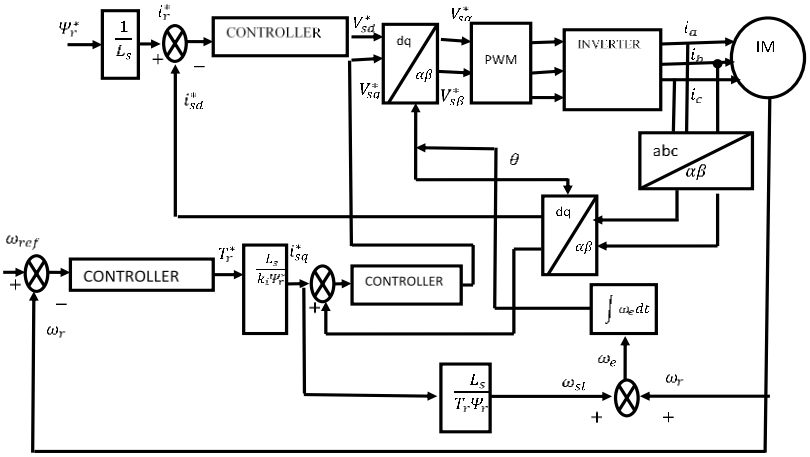

Fig. 1. Block diagram of IFOC of SCIM [25]

2.1 Design of Control Algorithms

Decoupling of an SCIM is a difficult task due to the interaction between the torque and fluxes. DC machine-similar performance can be obtained in SCIM only by decoupling of torque and flux technique, and this is the only where vector control is possible in SCIM [26-27]. Fig. 1 is the block diagram of the IFOC of SCIM. In this paper, PID controller and sliding mode controller are designed and are used individually integrated in the induction drive to vectorially control the speed at the stated operating condition. Their performance is compared using the speed response, measured in terms of the smoothness of the response [28-32]. The rotor speed ω_m is compared to rotor speed command $\omega_m{}^*$ and the resulting error is process in the controller. The controller generates the q axis reference current $i_{qs}{}^*$

Both d-q axis commands are compared to the d-q axis that is obtained from the transformation from equation (12).

$$\begin{bmatrix} i_{ds} \\ i_{qs} \end{bmatrix} = \begin{bmatrix} \cos\theta & \cos\left(\theta - \frac{2\pi}{3}\right) & \cos\left(\theta + \frac{2\pi}{3}\right) \\ -\sin\theta & -\sin\left(\theta - \frac{2\pi}{3}\right) & -\sin\left(\theta + \frac{2\pi}{3}\right) \end{bmatrix} \begin{bmatrix} i_a \\ i_b \\ i_c \end{bmatrix} \quad (12)$$

The current regulator output are $v_{ds}{}^*$ and $v_{qs}{}^*$ Through (13) the voltage command $v_{ABC}{}^*$ gives the input to PWM inverter.

$$\begin{bmatrix} v_a \\ v_b \\ v_c \end{bmatrix} = \begin{bmatrix} \cos\theta & -\sin\theta \\ \cos\left(\theta - \frac{2\pi}{3}\right) & -\sin\left(\theta - \frac{2\pi}{3}\right) \\ \cos\left(\theta + \frac{2\pi}{3}\right) & -\sin\left(\theta - \frac{2\pi}{3}\right) \end{bmatrix} \begin{bmatrix} v_{ds} \\ v_{qs} \end{bmatrix} \quad (13)$$

$$w_r = \int \frac{p}{2J}(T_e - T_L)$$

$$\theta_e = \int \omega_e dt = \int (\omega_{sl} + \omega_r) dt \,, \quad (14)$$

θ_e is the rotor flux angular position

$\omega_r = \frac{p}{2}\,\omega_m$, ω_{sl} is ths slip frequency

$$\omega_{sl} = \frac{L_m R_r i_{qs}}{\varphi_{dr} L_r} \quad (15)$$

Please arrange all equation numbers serially after equation number (15). Equation number (14), (15) & (16) are presented twice.

The input voltage to the three phase induction motor is shown in equation (16) to (19)

$$V_a = \sqrt{2} V_{rms} \sin(wt) \quad (14)$$

$$V_b = \sqrt{2} V_{rms} \sin\left(wt - \frac{2\pi}{3}\right) \quad (15)$$

$$V_b = \sqrt{2} V_{rms} \sin\left(wt + \frac{2\pi}{3}\right) \quad (16)$$

3. SLIDING MODE CONTROL

With a sliding mode controller, the system is controlled in such a way that the error in the system states always moves towards a sliding surface. The sliding surface is defined with the tracking error (e) of the state and its rate of change (e˙) as variables. The distance of the error trajectory from the sliding surface and its rate of convergence are used to decide the control input (u) to the system. The sign of the control input must change at the intersection of the tracking error trajectory with the sliding surface. In this way, the error trajectory is always forced to move towards the sliding surface.

Under the complete field-oriented control, the mechanical equation can be equivalently described as:

$$T_e = K_T i_{qs} \,, \quad (16)$$

K_T is constant torque

$$K_T = \frac{3PL_m}{4L_r}\varphi_{dr} \quad (17)$$

The mechanical equation of induction motor is

$$T_e = J\dot{\omega_m} + B\omega_m + T_L \quad (18)$$

From equation (16) and (18)

$$bi_{qs} = \dot{\omega_m} + a\omega_m + f \quad (19)$$

$$a = \frac{B}{J} \,, \; b = \frac{K_T}{J} \,, \; f = \frac{T_L}{J}$$

Equation (19) has Δa , Δb , Δf are uncertainties

$$\dot{\omega_m} = -(a + \Delta f)\omega - (a + \Delta f) + (b + \Delta b) i_{qs} \quad (20)$$

Tracking speed errors is defined as

$$e(t) = \omega_m(t) - \omega_m{}^*(t) \quad (21)$$

Where $\omega_m{}^*$ is the reference speed,

taking derivative of equation 21

$$\dot{e}(t) = \dot{\omega_m}(t) - \dot{\omega_m}{}^*(t) \quad (22)$$

Also,

$$\dot{e}(t) = -ae(t) + u(t) + d(t)$$

Where

$$u(t) = bi_{qs} - a\omega_m{}^*(t) - f(t) - \dot{\omega_m}{}^*(t) \quad (23)$$

And the uncertainties $d(t)$

$$d(t) = -\Delta a \omega_m(t) - \Delta f(t) + \Delta b i_{qs} \quad (24)$$

Sliding mode surface is equation (19)

$$s(t) = e(t) - \int_0^t (k - a) e(\tau) d\tau \quad (25)$$

Where k is a constant gain , whenthe slidng mode occur on the sliding surface,

then $s(t) = \dot{s}(t) = 0$, which amount to equation (26)

$$\dot{e}(t) = (k - a)e(t) \quad (26)$$

In order to obtain the speed trajectory tracking, k must be chosen so that the term $(k - a)$ is strictly negative and hence $k < 0$, therefore the sliding surface is defined as:

$$s(t) = e(t) - \int_0^t (k - a)e(\tau)d\tau = 0 \quad (27)$$

The variable structure controller is design as in equation 9,

$$u(t) = ke(t) - \beta sgn(S) \quad (28)$$

Where

β is a swtching gain, S is the sliding variable and $\text{sgn}(\text{S(t)})$ is the sign function defined as

$$\text{sgn}(\text{S(t)}) = \begin{cases} 1 & \text{if s(t)} > 0 \\ -1 & \text{if s(t)} < 0 \end{cases} \quad (29)$$

also, the gain β must be chosen so that $\beta \geq |d(t)|$all the time.

Please check the below highlighted part

Combining equation 18 and 21, we have

When sliding mode occurs on the sliding surface, then $S(t) = \dot{S}(t) = 0$ and the tracking error converges to zero exponentially. From (23) and (28), the current command $i_{qs}{}^{*}$ can be obtained as

$$i_{qs}{}^{*}(\text{t}) = \frac{1}{b}[ke - \beta sgn(S) + a\omega_m{}^{*}(\text{t}) + \dot{\omega_m}{}^{*}(t) + f\,] \quad (30)$$

and the value of the current sent to the motor from the controller is given in equation (23), for the command reference speed [33].

3.1 Reduction of Chattering

In a system, where modeling imperfection, parameter variations, and amount of noise are greater, the value of β must be large to obtain a satisfactory tacking performance with a sliding mode controller. But a larger value of β leads to more chattering of the control variable and system states. A boundary layer of definite width on both sides of the switching line is introduced to reduce chattering. If $\emptyset$ is the width of the boundary layer on either side of the switching line, as shown in Fig. 2. The control law of (28) is modified as:

$$u(t) = ke(t) - \beta sgn(\tfrac{s}{\emptyset}) \quad (31)$$

Where

$$sat\left(\tfrac{s}{\emptyset}\right) = \begin{cases} \frac{s}{\emptyset} & if \quad \text{IsI} \leq \emptyset \\ sgn(s) & if \quad \text{IsI} > \emptyset \end{cases} \quad (32)$$

The proposed flowchart for sliding mode controller is shown in Fig. 2.

3.2 Design of PID Controller

MATLAB tool is used to search efficiently for the optimal PID controller parameters within the system. This approach has superior features like easy implementation and less computational effort [28,34,35,36]. Fig. 3 shows the block diagram of the PID controller.

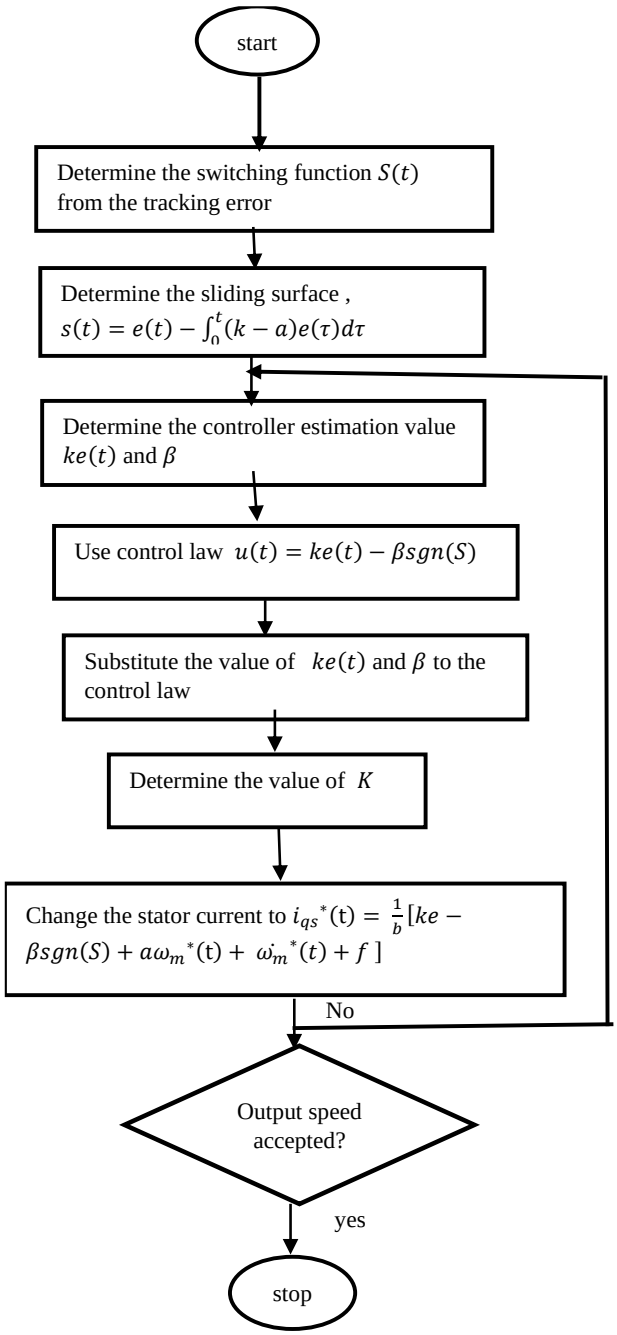

Fig. 2. Flow chat of sliding mode controller development

From Fig. 3, the output of the PID controller, *u (t)*, constitutes the sum of three signals: the signal obtained by multiplying the error signal by a constant proportional gain, k_p , the signal obtained by differentiating and multiplying the error signal by constant derivative gain, k_D, and the signal obtained by integrative control response. Defining $u(t)$ as the controller output, the final form of the PID algorithm is:

$$u(t) = k_p.e(t) + k_i \int e(t)dt + k_d \frac{de(t)}{dt} \quad (33)$$

The tuning mechanism is designed using a MATLAB tool that can derive the transfer function of the complex SCIM and vary the PID parameters to control the speed of the motor. After a successful tuning of the controller using the trial and error method, a fixed PID gain of $k_i = 1.3$, $k_p = 87.1$ and $k_D = 0.004$ were realized to arrive at best dynamic performance.

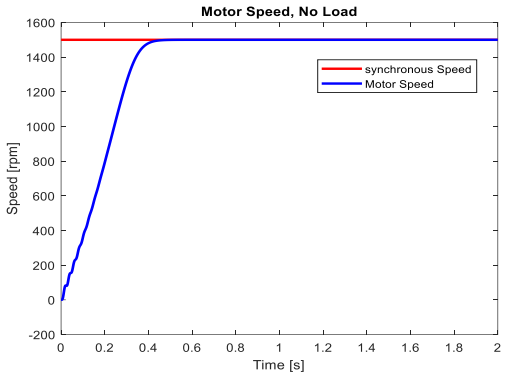

Fig. 3. Speed response of IM at no load

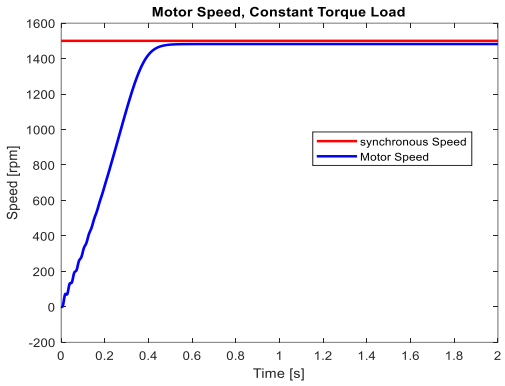

Fig. 4. Speed response of IM at 10Nm

4. RESULTS AND DISCUSSION

The performance of the SCIM with no load condition, and the results of the controllers (PID and sliding mode) with the stated operating conditions are presented in this section. The parameters of the tested motor are listed in Table 1. The design and simulation were carried out using MATAB Simulink. The controllers were separately designed for the varying speed control with constant load and intermittent load with a constant.

The speed, torque, and current responses of each controller were studied, analyzed, and compared in terms of steady state error, rise time, settling time, overshoot, and undershoot. The simulation results are subdivided in the subsequent sections.

Table 1. SCIM parameter

Motor parameters	specification
voltage	460
Power	2.5kW
Frequency	50Hz
Rotor Resistance	0.228Ω
Stator Resistance	0.087Ω
Rotor Inductance	0.8×10^{-3}
Stator Inductance	0.8×10^{-3}
Mutual Inductance	0.0347H
Pole	4
Initial	1.662Kgm^2
speed	1440RPM

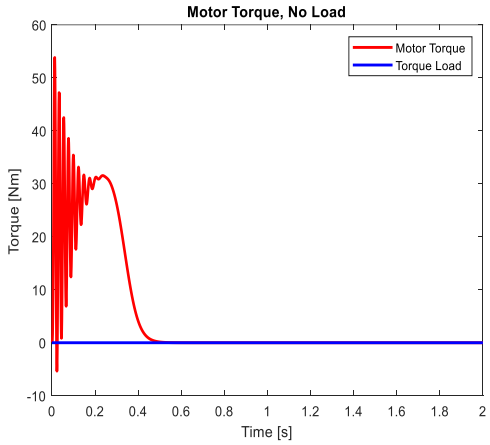

Fig. 5. Speed response with PID controller

4.1 Dynamic Performance of SCIM with without Controllers

The dynamic performance of the motor is shown in Fig. 3 through 6. Fig. 3 is the speed response of the motor without load, and the corresponding electromagnetic torque is presented in Fig. 5. The steady stated speed of the motor is 1500 rpm, having the same value as the synchronous speed because of the no-load situation. The speed response settled at 0.4 seconds, and that was its rise time. The speed response when a 10Nm load was applied is presented in Fig. 4, and its corresponding torque response is presented in Fig. 6. It is observed that the effect of the applied load has reduced the speed value from 1500 rpm to 1480 rpm. The induction motor drive is a constant speed drive; the rotor speed value depends on the slip. Hence, speed control of this drive becomes the basic requirement if it must be used for variable-speed applications. The speed control of the motor is presented in the subsequent sections using PID and sliding mode controllers.

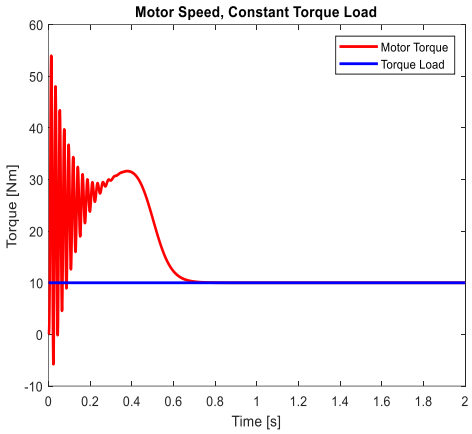

Fig. 6. Speed response with PID controller

4.2 Results under Variable Speed and Constant Load Torque Using PID Controller

Fig. 7 shows the speed performance of the SCIM with PID controller under variable speed (0 rad/sec, 10 rad/sec, and 25 rad/sec) and a constant load of 4 Nm. As shown in Fig. 7, the speed tracking ability of this model is fast, and it displays a good transient response. The response shows a variable speed of 0 rad/sec from 0 sec to 0.5 sec, 10 rad/sec from 0.5 sec to 1 sec, and finally, there was an increase in speed from 10 rad/sec to 25 rad/sec.

The speed response has an overshoot of 2.5% and an undershoot of 0%; the settling time, rise time, and steady state error are 0.05 sec, 0.03 sec, and 0.5 rad/s, respectively, when driving the load with 10 rad/sec. Also, the motor speed response has an overshoot of 12.%. and an undershoot of 0%. The settling time, rise time, and steady state error are 0.22 sec, 0.05 sec, and 8%, respectively, when driving the load with 25 rad/sec. The corresponding electromagnetic torque and current response are shown in Figs. 8 and 9, respectively. The torque response overshoots at every speed increase and settles after 0.3 sec, as seen in Fig. 12. Also, the current response in Fig. 9 overshoots at every increase in speed and settles immediately after 0.03 sec.

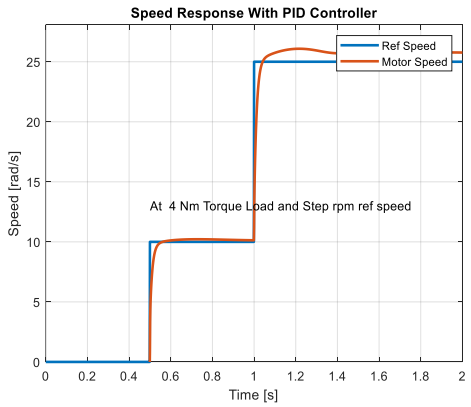

Fig. 7. Variable Speed response with PID controller

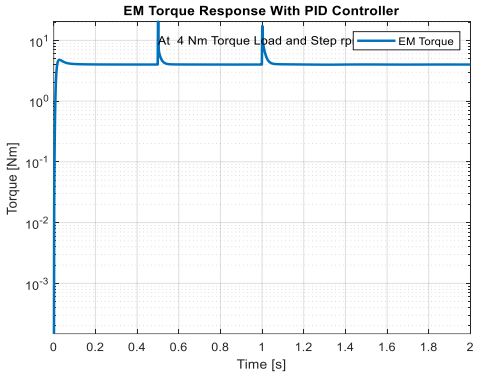

Fig. 8. Torque on variabel Speed response with PID controller

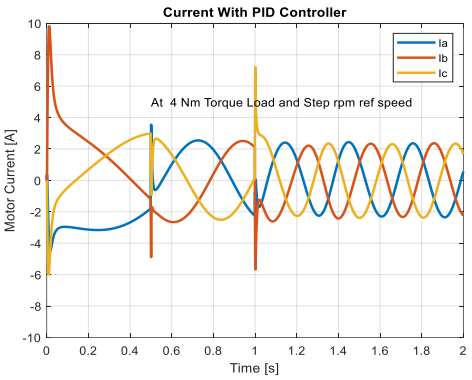

Fig. 9. Current on variabel Speed response with PID controller

4.3 Results under Variable Speed and Constant Load Torque Using SM Controller

Fig. 10 shows the speed performance of the SCIM with SM controller under variable speed (0 rad/sec, 10 rad/sec, and 25 rad/sec) and a constant load of 4 Nm. As shown in Fig. 10, the speed tracking ability of this model is fast, and it displays a better transient response compared to

the response of PID. The response shows a variable speed of 0 rad/sec from 0 sec to 0.5 sec, 10 rad/sec from 0.5 sec to 1 sec, and finally there was an increase in speed from 10 rad/sec to 25 rad/sec..

The speed response has an overshoot of 1.5.% and an undershoot of 0%; the settling time, rise time, and steady state error are 0.02 sec, 0.01 sec, and 0 rad/s, respectively, when driving the load with 10 rad/sec. Also, the motor speed response has an overshoot of 4% and an undershoot of 0%. The settling time, rise time, and steady state error are 0.05 sec, 0.01 sec, and 0.1%, respectively, when driving the load with 25 rad/sec. The corresponding electromagnetic torque and current response are shown in Figs. 11 and 12, respectively.

The torque response overshoots at every speed increase and settles after 0.3 sec as seen in Fig. 11. Also, the current response in Fig. 12 overshoots at every increase in speed.

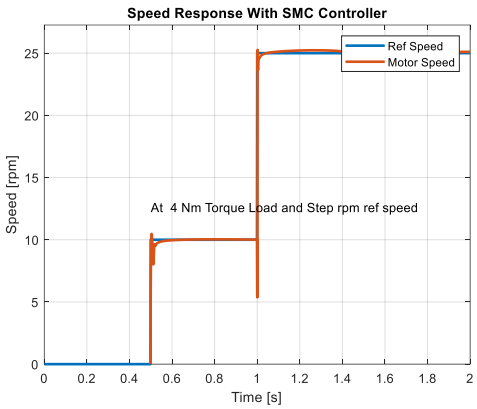

Fig. 10. Variable speed response with SM controller

The direct comparison of the controllers on the dynamic performance of the motor driving 4Nm with varying speeds of 0 rad/s, 10 rad/s, and 25 rad/s at 0 s, 0.5 s, and 1 s, respectively, is presented in Fig. 12. From Fig. 12, the SM controller gives a more superior performance. when compared to PID. The entire performance of these controllers under this operating condition is recorded in Table 2.

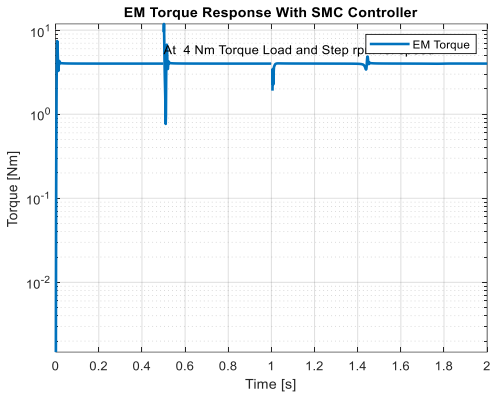

Fig. 11a. Torque response on variabel Speed with SM controller

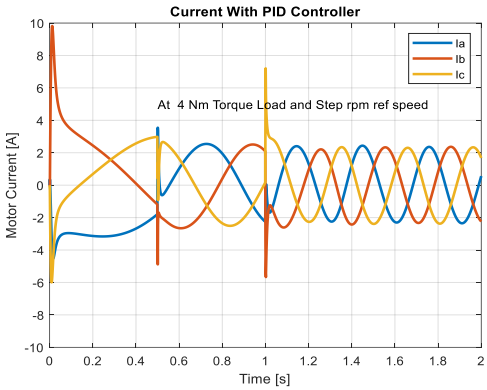

Fig. 11b. Current response on variable Speed with SM controller

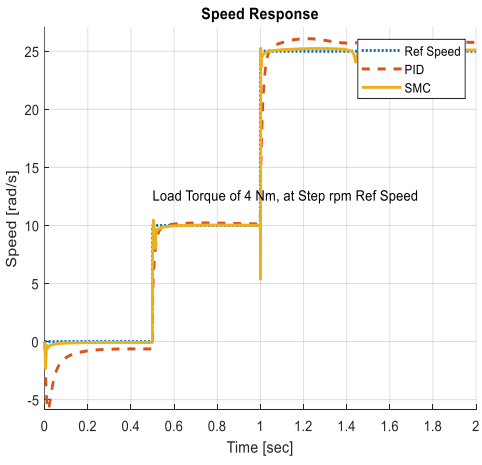

Fig. 12. Variable Speed response of PID and SM controller

Table 2. Performance comparison of controllers on Variable speed and Constant load torque

Control Parameters (10	Controllers

rad/Sec)	PID	SMC
Steady State Error [%]	4	0.1
Overshoot [%]	6	2
Rise Time	0.05	0.01
Settling Time	0.22	0.02
Control Parameters (25 rad/Sec)	**Controllers**	
	PID	**SMC**
Steady State Error [%]	8	0.1
Overshoot	12	4
Rise Time	0.05	0.01
Settling Time	0.22	0.05

4.4 Results under Intermittent Loads with Constant Speed Using PID Controller

Fig. 13 shows the speed performance of the SCIM with PID controller under an intermittent load (0 Nm, 4 Nm, and 9 Nm) and constant speed of 25 rad/sec. As shown in Fig. 11, the speed-tracking ability of this model is fast with the external disturbance. The response shows the speed response of 0 Nm and the load of 4 Nm and 9 Nm are introduced at 0.5 sec and 1 sec, respectively. The speed response has an overshoot of 16.%; the settling time, rise time, and steady state error are 0.2 sec, 0.02 sec, and 2%, respectively, when driving 4Nm. Also, the motor speed response has an overshoot of 0%; the settling time, rise time, and steady state error are 0.4 sec, 0.02 sec, and 1.5%, respectively, when driving 9Nm. The corresponding electromagnetic torque and current response are shown in Figs. 14 and 15, respectively. The torque response overshoots at every load increase and settles after 0.1 sec, as seen in Fig. 14. Also, the current response in Fig. 15 overshoots at every increase in speed and settles immediately after 0.02 sec.

4.5 Results under Intermittent Loads with Constant Speed Using SM Controller

Fig. 16 shows speed performance of the SCIM with SM controller under an intermittent load (0 Nm, 4Nm and 9Nm) and constant speed of 25rad/sec. As shown in Fig. 11, speed tracking ability of this model is faster with the external disturbance compare to PID controller. The response shows the speed response of 0 Nm and the load of 4Nm and 9Nm are introduced at 0.5 sec and 1 sec respectively.

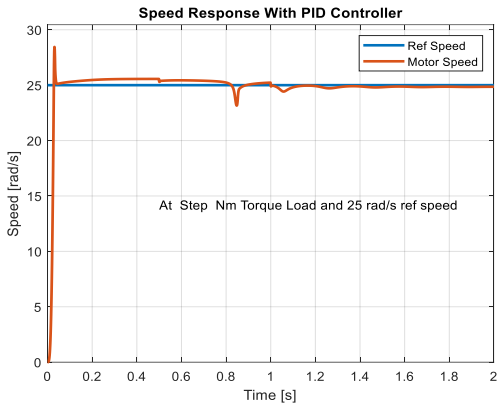

Fig. 13. Speed response on intermittent load with PID controller

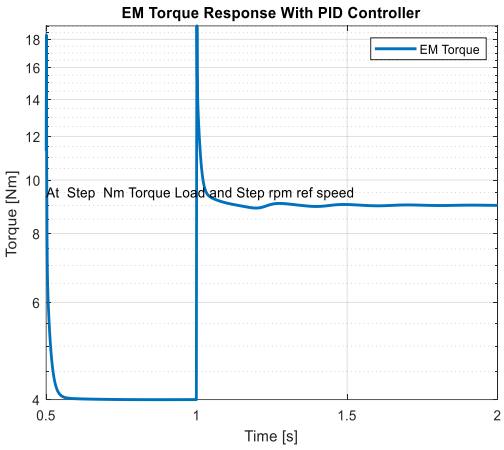

Fig. 14. Torque response on intermittent load with PID controller

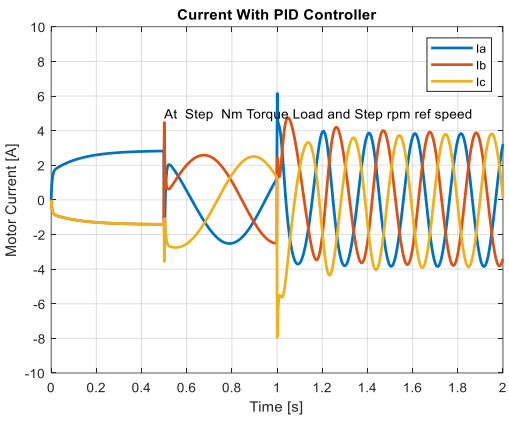

Fig. 15. Current response on intermittent load with PID controller

The speed response has overshoot of 0%, the settling time, rise time and steady state error are 0.01 sec, 0.02 sec, and 0.1%, respectively when driving 4Nm. Also, the motor speed response

has overshoot of 0 %, the settling time, rise time and steady state error are 0.1%, 0.02 sec, and 0.1% respectively when driving when driving 9Nm. The corresponding electromagnetic torque and current response are shown in Figs. 17 and 18, respectively. The torque response overshoots at every load increase and settles after 0.1 sec as seen in Fig. 1. Also, the current response in Fig. 11 overshoots at every increase in speed and settles immediately after 0.02 sec.

The direct comparison of the controllers on the dynamic performance of the motor driving intermittent loads of 4 Nm and 9 Nm with a constant speed of 25 rad/s is presented in Fig. 19. From Fig. 19, the SM controller gives a more superior performance when compared to the PID. The entire performance of these controllers under this operating condition is recorded in Table 3.

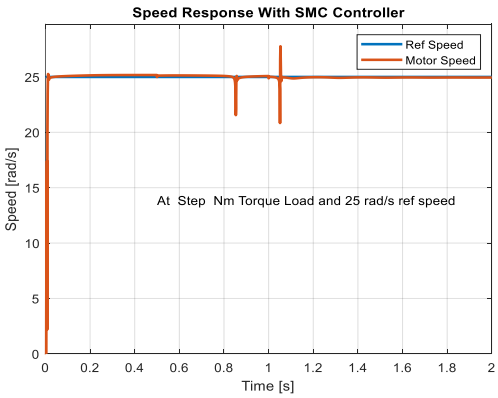

Fig. 16. Speed response on intermittent load with SM controller

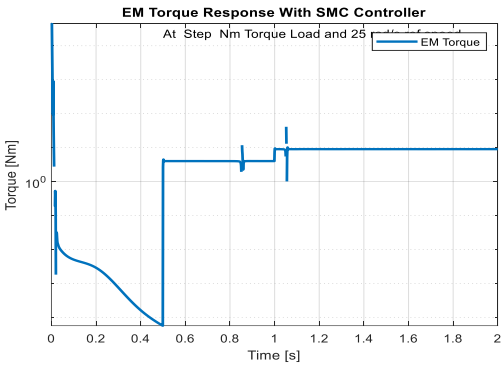

Fig. 17. Torque response on intermittent load with SM controller

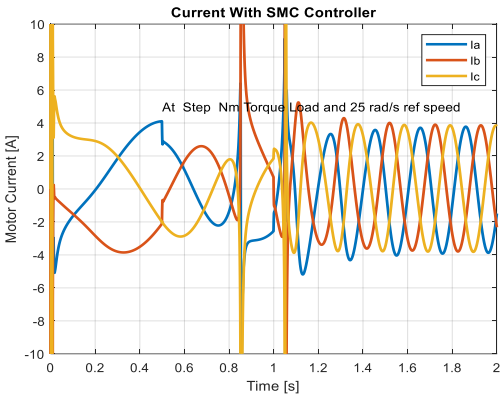

Fig. 18. Current response on intermittent load with SM controller

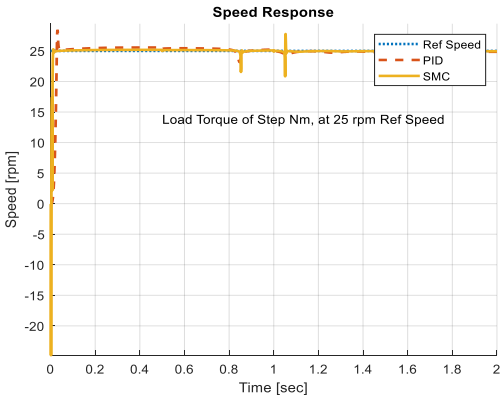

Fig. 19. Speed response of PID and SM controller on intermittent loading

Table 3. Performance comparison of controllers on Constant speed and intermittent load torque

Control Parameters (4Nm)	Controllers	
	PID	SMC
Steady State Error [%]	2	0.1
Overshoot [%]	16	0
Rise Time (sec)	0.02	0.02
Settling Time (sec)	0.2	0.02
Control Parameters (9Nm)	**Controllers**	
	PID	**SMC**
Steady State Error [%]	1.5	0.1
Overshoot [%]	0	16
Rise Time (sec)	0.02	0.02
Settling Time (sec)	0.4	0.01

5. CONCLUSION

This paper has presented the speed control of SCIM using the vector control technique with PID and SM controllers. In this work, the flux and torque components were controlled separately in

the d-axis and q-axis through the decoupling method. The simulation results of the SCIM drive model include the stator current, rotor speed, and electromagnetic torque under constant load torque using variable speed intermittently.

The speed characterization of each controller is presented using their steady state error, rise time, settling time, percentage overshoot, and undershoot. The values of these performance parameters are recorded in Tables 2 and 3. From simulation results, it testifies that the SC controller gave the best improved speed response. The model has given a much better speed-enhanced performance when compared to the results from Umoette et al. [1], Nazeer and Shahina [21], and Singha et al. [37] where the steady state error and settling time are higher compare to what is realized in this work. Also, the work has given the needed attention in SCIM low-speed analysis. The proposed model will be useful in mechatronics and robotics where high precision and smooth speed control are paramount.

DISCLAIMER (ARTIFICIAL INTELLIGENCE)
Please write this section
Option 1:

Author(s) hereby declare that NO generative AI technologies such as Large Language Models (ChatGPT, COPILOT, etc) and text-to-image generators have been used during writing or editing of this manuscript.

Option 2:

Author(s) hereby declare that generative AI technologies such as Large Language Models, etc have been used during writing or editing of this manuscript. This explanation will include the name, version, model, and source of the generative AI technology and as well as all input prompts provided to the generative AI technology.

Details of the AI usage are given below:

1.
2.
3.

COMPETING INTERESTS

Authors have declared that no competing interests exist.

REFERENCES

1. Umoette AT, Okoro OI, Davidson IE. Performance analysis of a 10hp three phase induction motor using classical and finite-elements for varying load conditions. 2021 IEEE PES/IAS Power Africa. 2021;1-5.
2. Umoette AT, Okoro OI, Davidson IE. Implementation of indirect field oriented control of a 2.2kw three-phase induction motor using MATLAB Simulink. 2021 IEEE AFRICON. 2021;1-6.
3. Kimiaghalam B, Rahmani MI, Halleh H. Speed & torque vector control of induction motors with Fuzzy logic controller. In IEEE Control, Automation and Systems. 2008;360-366.
4. Umoette AT, Okoro OI, Davidson IE. Speed performance enhancement and analysis of a three phase induction motor driving a pump load using vector control technique. 2022 IEEE PES/IAS Power Africa, Kigali, Rwanda. 2022;1-5.
5. Haddoun M, Benbouzid EH, Diallo D, Abdessemed R, Ghouili J, Srairi K. Comparative analysis of control techniques for efficiency improvement in elective vehicles. In Proc. IEEE Vehicle Power Propulsion Conf. 2007;629–634.
6. Angalalli A, Bapiraju JV. Analytical model for real-time simulation of low voltage induction motor drive. In 2017 IEEE International Electric Machines and Drives Conference (IEMDC), Miami, FL; 2017.
7. Hussain S, Bazaz MA. Review of vector control strategies for three phase induction motor drive. 2015 International Conference on Recent Developments in Control, Automation and Power Engineering (RDCAPE); 2015.
8. Yin Z, Du C, Liu J, Sun X, Zhong Y. Research on auto disturbance-rejection control of induction motors based on an ant colony optimization algorithm. IEEE Trans. Ind. Electron. Apr. 2018;65(4):3077-3094.
9. Tiwari R, Chatterji S. Comparative analysis of vector control of induction motor using PI controller with fuzzy logic controller. International Journal of Science and Research (IJSR). April 2013;2(4):404-409.
10. Goman V, Prakht V, Kazakbaev V, Dmitrievskii V. Comparative study of induction motors of IE2, IE3 and IE4 efficiency classes in pump applications taking into account CO2 emission intensity. Applied Sciences. MDPI; 2020.

11. Umoette AT, Okoro IO, Abunike E. Performance enhancement of 2.5kW induction motor drive using novel hybridized control algorithm'. American Journal of Engineering Research (AJER). 2024;13(8):47-61.
e-ISSN: 2320-0847
p-ISSN: 2320-0936
12. Wang H, Yang Y, Ge X, Zuo Y, Yue Y, Li S. PLL- and FLL-based speed estimation schemes for speed-sensorless control of induction motor drives: Review and new attempts. In IEEE Transactions on Power Electronics. March 2022;37(3):3334-3356.
13. Umoette AT, Mbetobong UF, Ubom EA. Development of site-specific optimal tilt angle model for fixed tilted plane PV installation in Akwa Ibom State, Nigeria. Science Journal of Energy Engineering. 2016;4(6):50-55.
14. Umoette AT, Udofia JP, Ubom EA. Energy audit and standalone solar power generation design for Akwa Ibom State University Main Campus. International Multilingual Journal of Science and Technology (IMJST). June – 2023;8(6).
ISSN: 2528-9810
15. Silas AF, Umoette AT, Ekanem BD. Energy analytical model for the selection of peak sun hour and days of power autonomy for PV solar power system components sizing. Journal of Multidisciplinary Engineering Science and Technology (JMEST). March – 2024;11(3).
ISSN: 2458-9403
16. Umoette AT, Silas AF, Kingsley BC. Clearness index–based computation and evaluation of mean daily insolation and optimal fixed tilt angle for PV installation in Uyo, Akwa Ibom State. International Multilingual Journal of Science and Technology (IMJST). March – 2024;9(3).
ISSN: 2528-9810
17. Hannan MA, Ali JA, Mohamed A, Amirulddin UAU, Tan NML, Uddin MN. Quantum-behaved lightning search algorithm to improve indirect field-oriented fuzzy-PI control for IM drive. In IEEE Transactions on Industry Applications. July-Aug. 2018;54(4):3793-3805.
18. Amarnath KR. Variable refrigerant flow: Demonstration of efficient space conditioning technology using variable speed drives. Electric Power Research Institute (EPRI) Report 1018446; 2018.
19. Oliveira F, Uki A. Comparative performance analysis of induction and synchronous reluctance motors in chiller systems for energy efficient buildings. IEEE Transactions on Industrial Informatics. August 2019;15(8).
20. Sahu SK, Neem DD. A robust speed sensorless vector control of multilevel inverter fed induction motor using particle swarm optimization. International Journal of Innovative Research in Electrical, Electronics, Instrumentation, and Control Engineering. January 2015;3(1).
21. Nazeer N, Shahina TN. Speed control for indirect vector control of induction motor drives at low speeds. IEEE Transactions on Energy, Communication, Data Analytics and Soft Computing. Sept. 2019;1111-1118.
22. Eissa MM, Virk GS, Abdei AM, Ghith ES. Optimum induction motor speed control technique using particle swarm optimization. International journal of Engineering. 2013;3:65-73.
23. Jayashri W, Swapnil Z, Rahul S. Review of various methods in improvement in speed, power & efficiency of induction motor. IEEE Transactions on Energy, Communication, Data Analytics and Soft Computing. 2017;5(17):3293-3297.
24. Souad C, Latifa A, Larbi C, Aloalu C, Said D. Optimized torque control via back stepping using genetic algorithm of induction motor. Journal for Control, Measurement, Electronics, Computing and Communications. 2017;57(2):379-386.
25. Ahmad I, Tripathi RK. Indirect field-oriented control (IFOC) of induction motor using SPVPWM fed with Z-souce inverter. IEEE Conference on Engineering and System. 2012;1-5.
26. Madhavi L, Mhaisgewal SI. Induction motor speed control using PID controller. International Journal of Technology and Engineering Science. 2013;1(2):151-155.
27. Pravallika S, Chandra JN, Reddy DP. Optimization of speed control of induction using self-tuned PI plus hybrid controller. Internation Journal of Emerging Technology and Advanced Engineering. 2015;5(1).
28. Blashke F. The principle of field orientation as applied to the new transvector closed loop control system for rotating field machines. Siemens Rev. May 1972;39(5): 217-220.
29. Stephen O, Ejiofor N, Abuch NC, Damian N, Okoro OI. Performance study of three-phase induction motor driving a load. Analysis Article Discovery; 2019.
ISSN 2278–5469

eISSN 2278–5450.
30. Bhola J, Panda M, Pandey PK, Pan L. PSO-based online vector controlled induction motor drives. IEEE International Conference on Electrical, Electronics, and Optimization Techniques (ICEEOT). 2016;2234-2240.
31. Fattah JA, Ikhlass PE. Performance and comparison analysis of speed control of induction motors using improved hybrid PID-Fuzzy controller. CES Transactions on Electrical Machines and Systems. 2015;2(2):575-581.
32. Zicheng L, Yongdong L, Zheng Z. A review of drive techniques for multiphase machines. CES Transactions on Electrical Machines and Systems. 2018;2(2):243-251.
33. Fizatul AP, Marizan S, Zulkifilie I. Performance of sliding mode control for three phase induction motor. Conference of Science and Social Reseach, Malaysia; 2010.
34. Cheng S, Gong B, Wang JA. Novel hybrid speed controller of the vector control system. International Conference on Control, Automation and Systems 2010, Oct. 27-30, 2010 in KINTEX, Gyeonggi-do, Korea.
35. Mohan H, Pathak MK, Dwivedi SK. Reactive power based speed control of induction motor drive using fuzzy logic for industrial applications. IEEE International Conference on Power Electronics, Smart Grid and Renewable Energy (PESGRE2020); 2020.
36. Yang Z, Lu C, Sun X, Ji J, Ding Q. Study on active disturbance rejection control of a bearingless induction motor based on an improved particle swarm optimization–genetic algorithm. In IEEE Transactions on Transportation Electrification. June 2021; 7(2):694-705.
37. Singha AK, Chaturvedib DK, Palc NK. PSO based fractional order PID controller for speed control of induction. International Conference on Power Energy, Environment and Intelligent Control (PEEIC); 2019.